The molecular basis of genetic interaction diversity in a metabolic pathway

Harry E. Kemble[1,2], Catherine Eisenhauer[1], Alejandro Couce[1,3], Audrey E. Chapron[1], Mélanie A. Magnan[1], Gregory Gautier[4,5], Hervé Le Nagard[1], Philippe Nghe[2], Olivier Tenaillon[1*]

[1]Infection, Antimicrobials, Modelling, Evolution, INSERM, Unité Mixte de Recherche 1137, Université Paris Diderot, Université Paris Nord, 75018 Paris, France

[2]École Supérieure de Physique et de Chimie Industrielles de la Ville de Paris (ESPCI Paris), PSL Research University, UMR CNRS-ESPCI CBI 8231, 10 Rue Vauquelin, 75231 Paris Cedex 05, France

[3]Department of Life Sciences, Imperial College, London, SW7 2AZ, UK

[4]Centre de Recherche sur l'Inflammation, INSERM, UMRS 1149, 75018 Paris, France

[5]Laboratoire d'Excellence INFLAMEX, Université Paris Diderot, Sorbonne Paris Cité, 75018 Paris, France

Metabolic imbalances underlie a large spectrum of diseases, spanning congenital and chronic conditions and cancer[1]. Our ability to explain and predict such imbalances remains severely limited by the diversity of underlying mutation effects and their dependence on the genetic background and environment[2–6], but it is unclear whether these complicating factors can be reduced to simple quantitative rules. Here, we characterise their interplay in determining cell physiology and fitness by systematically quantifying almost 4,000 interactions between expression variants of two genes from a classical sugar-utilisation pathway containing a toxic metabolite in the model bacterium, *Escherichia coli*, in different environments. We detect a remarkable variety of types and trends of intergenic interaction in this linear pathway, which cannot be reliably predicted from the effects of each variant in isolation, along with a dependence of this epistasis on the environment. Despite such apparent complexity, the fitness consequences of interactions between alleles and environment are explained by a mechanistic model accounting for catabolic flux and toxic metabolite concentration. Our findings reveal how, contrary to a common assumption[7–13], the nature of fitness interactions is governed by more than just the topology of the molecular network underlying a selected trait. Our prospects of predicting disease and evolution will therefore improve by expanding our knowledge of the links among proteome, metabolome and physiology[14].

Organismal traits are the manifestation of complex molecular interaction networks spanning multiple scales of biological organisation, which themselves interact with the environment[15]. The rise of omics technologies is enabling increasingly detailed structural models of these networks[16], offering hope that gene interactions underlying important traits might be directly deduced from their topologies[7–13]. Direct measurements supporting this hypothesis are

however limited to one[10,17,18], or occasionally a few[18], variants of each gene (typically deletions). To examine whether such predictability applies more generally, we developed an experimental system with which to characterise the interactions between many alleles of two metabolic genes, along with their dependence on environmentally modulated gene expression, a common non-genetic mechanism for the modification of traits[5,19].

Our system was composed of two genes, *araA* and *araB*, encoding the enzymes responsible for the first two steps of *E. coli* L-arabinose catabolism[20]: L-arabinose isomerase (AraA) and L-ribulokinase (AraB), who together transform L-arabinose into the intermediate, L-ribulose-5-phosphate (Fig. 1a). L-ribulose-5-phosphate enters the pentose phosphate pathway (PPP) of central metabolism *via* further enzymatic reactions, ultimately supporting cell growth, but is itself toxic to *E. coli*, retarding growth when it accumulates[21]. Environmental modulation of gene expression was achieved by placing each of the two genes under an independent, chemically inducible promoter (Supplementary Methods).

For each promoter, 36 single-base variants were constructed, along with the initial "wildtype" sequence, and combined with all variants of the other promoter (Fig. 1b). The ultimate phenotype, competitive fitness, was then measured for the entire set of 1,369 genotypes under three different inducer concentration combinations (Figs. 1c-d; Supplementary Methods; Supplementary Tables 1-5). Fitness was measured by tagging the mutant library with molecular barcodes (tens to thousands per genotype) (Extended Data Figures 1 and 2), culturing the pooled library for ~30 mean generations, and tracking barcode frequencies over time with Next-Generation Sequencing (Extended Data Figure 3). The barcodes act as internal replicates for every genotype, enabling precise fitness estimates at high-throughput

(log relative fitness, F^{rel}, median standard deviation of 0.0011 for single mutants and 0.0047 for double mutants; Extended Data Figure 4).

The overall distribution of fitness effects depended critically on the inducer environment (Fig. 2a; Extended Data Figure 5a; Supplementary Table 6): most mutants were fitter than the wildtype in Env_1 (88% beneficial, median F^{rel} = 0.12), most were less fit in Env_2 (88% deleterious, median F^{rel} = -0.12), and about half were fitter and half were less fit in Env_3 (44% and 51%, respectively; median F^{rel} = -0.03). The correlation between fitness effects in different environments varied from strongly positive (Env_1-Env_3, Pearson's r=0.74, $p<2.2x10^{-16}$) to weakly positive (Env_2-Env_3, Pearson's r=0.26, $p<2.2x10^{-16}$) and weakly negative (Env_1-Env_2, Pearson's r=-0.11, $p=1x10^{-4}$) (Extended Data Figure 5b), demonstrating that genotype fitness in one environment can be an extremely poor predictor of fitness in other environments. At the level of individual alleles, all but one had changing patterns of effects across environments (Fig. 2b). In some environments, they were universally beneficial or deleterious across genetic backgrounds, and in others they switched between being beneficial and deleterious depending on the allele at the second promoter. This pervasive and inconsistent variability poses a clear challenge for the prediction of mutation effects.

To characterise the context-dependency of mutation effects, we examined the sign, strength and type[22] of intergenic fitness epistasis arising between the set of *araA* and *araB* promoter variants in each environment (Fig.3a, Extended Data Figure 6a). These all depended both on the environment and on the sign of the fitness effects of the two interacting mutations. Of all mutation pairs for which epistasis could be computed, the fraction exhibiting any kind of significant interaction varied from 89% (Env_1) to 81% (Env_3) and 39% (Env_2). Beneficial

pairs tended to interact negatively (89%, 72% and 100% of all significant interactions in Env_{1-3}, respectively), and deleterious pairs, positively (100% (1/1), 97% and 98%, respectively), a trend of *antagonism* reported for several other systems[23]. Interactions between beneficial and deleterious mutations could be mostly positive or mostly negative, depending on the environment and on which gene carried the beneficial/deleterious mutation. This epistatic diversity extended to individual mutation pairs, with more than 20% interacting both positively and negatively across environments (Extended Data Figures 6b and 6c). Concerning epistasis type (Fig. 1d), sign epistasis, which occurs when the sign of a mutation effect changes in the presence of a second mutation, represented 31% of significant interactions in Env_1, 17% in Env_2 and 34% in Env_3. Negative sign epistasis was even more frequent among beneficial mutations, comprising 35% of significant interactions between them in Env_1, 33% in Env_2 and 60% in Env_3. Importantly, some kinds of interaction arose in only one or two environments (*eg*. negative reciprocal sign epistasis), suggesting a critical role for the environment in determining possible genetic interactions.

Confronted with such a variety of interactions, we asked whether they might be quantitatively understood in terms of the fitness effects of the interacting mutations, as has been found for some other mutation sets[24]. We found that the effects of individual mutations were weakly predictive of the type and value of epistasis they exhibited with mutations at the second promoter (Fig. 3a scatterplots). In all environments, there was a significantly negative correlation between the sum of individual fitness effects and the value of epistasis (Pearson's $r = -0.36, -0.37, -0.51$ in Env_{1-3}, respectively; $p < 2.2 \times 10^{-16}$ for all), a trend of *diminishing returns* that appears common across experimental systems[24] (Extended Data Figure 7a). However, when the two genes were considered separately, the relationship between individual fitness effects and epistasis was found to be markedly different between *araA* and

araB: the negative correlation was stronger for $P_{LtetO\text{-}1}$-*araA* mutations being added to existing $P_{LlacO\text{-}1}$-*araB* mutations than for the inverse case (Extended Data Figures 7b and 7c; Pearson's $r = -0.67, -0.73, -0.63$ in $Env_{1\text{-}3}$, $p < 2.2\text{x}10^{-16}$ for all, *vs.* 0.12, -0.20 and -0.34, $p < 1.6\text{x}10^{-5}$ for all), in which the correlation can even be positive, an extremely rare trend in existing studies[24]. Moreover, we found that the average trend was in some cases strikingly non-monotonic (Extended Data Figures 7b and 7c), revealing that different alleles of a particular promoter can cause similar fitness changes on their own but interact very differently with alleles at the second promoter.

The relationship between individual mutation effects and epistasis was further complicated by the fact that it could be different for different alleles of the *same* promoter. For example, in Env_1, it is the numerous individually beneficial $P_{LtetO\text{-}1}$-*araA* mutations which cause the average negative trend with $P_{LlacO\text{-}1}$-*araB* background fitness, with many of them even becoming deleterious in high-fitness backgrounds. The rare individually deleterious $P_{LtetO\text{-}1}$-*araA* mutations behave differently, however, with certain of them causing a fairly consistent reduction in fitness regardless of the background (Fig. 3b, top panel). For individual $P_{LlacO\text{-}1}$-*araB* mutations in $P_{LtetO\text{-}1}$-*araA* backgrounds, the relationship was consistently non-monotonic, but had a different average direction for individually beneficial or deleterious alleles (Fig. 3b, bottom panel). Moreover, the trend for a given allele could vary greatly with the environment (Extended Data Figures 7b and 7c). These results demonstrate that genes interacting simply through their common participation in a linear pathway can exhibit complex, allele- and environment-dependent trends of epistasis. The smooth patterns exemplified by Fig. 3b, however, suggest that they may in principle be understood from an underlying phenotypic mechanism.

144

145 To this end, we constructed a quantitative model of the metabolic pathway, where fitness
146 results from a balance between the benefit of catabolic flux[25] and the costs of intermediate
147 toxicity[26,27] and AraA and AraB protein expression[28]. Each promoter mutation was then
148 characterised as a change in the controlled expression of AraA or AraB. Because most
149 mutations lay outside of the repressor binding sites governing promoter inducibility (Fig. 1b),
150 the fold-change in enzyme expression/activity caused by each mutation was kept constant
151 across inducer environments. Parameters describing the fitness function, wildtype activities in
152 the 3 environments and expression effects of individual mutations were then optimised to
153 match the observed data (Supplementary Table 7; Extended Data Figure 8a).

154

155 The fitted model is in excellent agreement with our data, yielding r^2 values of 0.98 between
156 experimental and simulated fitness effects and 0.82 between experimental and simulated
157 epistasis coefficients (fig. 4a; Extended Data Figure 8b; see Extended Data Figure 9 for
158 alternative models). There is only one allele whose qualitative behaviour across environments
159 is not well captured by the model (Extended Data Figure 8b): G7A of $P_{LtetO-1}$-*araA*,
160 interestingly the only one conferring a directionally consistent fitness effect across all
161 environments (Fig. 2b), presumably because the direction of its effect on *expression* depends
162 on inducer concentration (supported by the fact that the mutated position overlaps the
163 repressor binding site (Fig. 1b)). Notably, the model is capable of recapitulating the diverse
164 and complex trends of epistasis seen in the data (Fig. 4b, Extended Data Figure 8c). In
165 particular, we find that the non-monotonic relationships between single-mutant fitness and
166 the fitness impact of alleles at the second promoter are well explained by the single mutants
167 lying at two sides of a phenotypic optimum (Fig. 4b). This is a relatively common

168 phenomenon in our dataset, mostly because L-ribulose-5-phosphate toxicity results in a
169 particular flux being optimal for fitness[26,27] (Extended Data Figure 10). Two alleles of the
170 same gene may thus result in similar fitness changes individually but cause substantially
171 different expression levels and fluxes, resulting in different interactions with mutations in the
172 second gene. This is principally due to enzymes possessing different degrees of flux control
173 on each side of the optimum, with lower levels of one resulting in the second having less
174 control.

175

176 The model reveals how the biology underlying a linear pathway can result in heterogeneous,
177 environmentally dependent intergenic interactions. When fitness depends solely on flux[25,27],
178 as is assumed in Flux Balance Analysis[29], the nature of epistasis should be guaranteed by
179 pathway topology alone[27]. Under the slightly more complex selection pressure resulting from
180 metabolite toxicity[26,27] and gene expression costs, however, interactions can be both
181 antagonistic and synergistic[27]. We find that epistatic categories form several localised zones
182 over the fitness landscape, their size and position dependent on the wildtype phenotype, in
183 turn controlled by the environment (Fig. 4c; Extended Data Figure 8d). In a smooth landscape
184 such as this, sign epistasis can occur when there is an overshoot[30] of the phenotypic optimum
185 in one (simple) or both (reciprocal) planes. Encouragingly, epistatic zones are generally large
186 and orderly enough to make the type of interaction experienced by two mutations in different
187 environments predictable, but only through knowledge of the underlying landscape and the
188 position of the relevant genotypes within it.

189

190 The importance of this knowledge becomes immediately apparent when considering the
191 existence of a disease threshold below a certain fitness (Fig. 4d). The two alleles shown can

lead to disease, but only when they co-occur, and only in one particular environment. The model thus provides a mechanism by which potential physiological defects can be manifested, aggravated or alleviated by particular combinations of alleles and environments[2–5]. Insight into intergenic fitness landscapes for other biological systems, and for genes connected by more complex topologies, will be indispensable for progress across medicine, bio-engineering and evolution.

Methods

Plasmid construction

Our library creation strategy depended on two plasmids, pKH1511c and pKH1511d, which were created in this study. pKH1511c serves as the library "backbone", carrying all the necessary elements of the final plasmid library except for the $P_{LtetO-1}$ and $P_{LlacO-1}$ promoters destined to drive *araA* and *araB* expression, respectively: *p15A* origin-of-replication, *lacI-tetR* repressor cassette (for inducibility of $P_{LtetO-1}$ and $P_{LlacO-1}$), *araA* and *araB*. *araA* and *araB* ORFs (with their upstream ribosome binding site-containing regions) are divergently oriented (with each followed by an artificial transcriptional terminator), and are separated by 2 restriction sites to allow easy insertion of divergently oriented $P_{LtetO-1}$ and $P_{LlacO-1}$ promoters. pKH1511d serves as a template for amplification of a *bsd* blasticidin S-resistance cassette with primers containing the $P_{LtetO-1}$ and $P_{LlacO-1}$ variant sequences, allowing their eventual insertion into pKH1511c (Extended Data Figure 1). pKH1511d replication is pir-dependent, abolishing the occurrence of false-positive colonies caused by PCR template carryover during library cloning. Plasmids, DNA fragments, PCR primers and bacterial strains used in the construction of these two plasmids are detailed in Supplementary Tables 1-4, respectively, and detailed cloning methods are provided in Supplementary Methods.

Strain engineering/adaptation

The final library host strain, *E. coli* MG1655 Δ*araBA* D-ara$^{+/evo}$ Δ*fucK* Δ*lacIZYA*::*cat* D/L-ara^{evo} (Supplementary Table 4), was originally designed to possess a rewired D-arabinose metabolism[31–33], in which *araB* (but not *araA*) participates. D-arabinose was not used in this

study, however, so this feature (D-ara$^{+/evo}$ Δ*fucK*) is not relevant here. In addition, *araA* and *araB* ORFs were removed from the chromosome, to allow them to be expressed exclusively from plasmids (the 3rd gene of the *araBAD* operon, *araD*, was kept on the chromosome under the control of its native L-arabinose-responsive promoter, as were the transcriptional regulator gene, *araC*, and the transporter genes, *araE*, *araFGH* and *araJ*; given the all-or-nothing response of the positive feedback loop governing L-arabinose uptake, all these genes are expected to be maximally induced by internal L-arabinose by the time of fitness measurement[34]). Further, *lacIZYA* was replaced by a *cat* chloramphenicol-resistance cassette. This allows the use of IPTG to control the artificial promoter, $P_{LlacO-1}$, in the absence of any effects resulting from induction of the native *lac* operon, and the absence of *lacY* also causes this control to be titratable rather than all-or-nothing[35]. Finally, this strain was transformed with plasmid pKH1503a (which carries an *araBA* cassette under the control of $P_{LlacO-1;}$ Supplementary Table 1) and briefly adapted to M9 with alternating D-/L-arabinose (see above) in the presence of a low concentration of IPTG. This adaptation step was included to allow fixation of any mutations conferring a very high fitness advantage to our engineered strain in our approximate experimental conditions, to avoid them interfering with mutant library competition experiments. Detailed strain engineering methods are provided in Supplementary Methods.

Library creation strategy

On the evolutionary scale, direct changes in the total cellular activity of a particular enzyme can occur through either regulatory mutations, which alter the concentration of active enzyme, or structural mutations, which can effect both active enzyme concentration and kinetic parameters. A common target of regulatory mutations is the promoter[36], which

controls a protein's expression level by determining transcription rate, and we decided to focus on promoter mutations in this study. We first placed *araA* and *araB* under the control of the well-known artificial, chemically-inducible promoters, $P_{LtetO-1}$ and $P_{LlacO-1,}$ developed by Lutz and Bujard[37]. They are each regulated by a single transcription factor (*tetR* repressor for $P_{LtetO-1}$ and *lacI* repressor for $P_{LlacO-1}$), and can be specifically induced to different levels by addition of a small, non-metabolisable compound (aTc for $P_{LtetO-1}$ and IPTG for $P_{LlacO-1}$). We focussed mutagenesis on the RNA polymerase-binding sites (-35 and -10 hexamers) of the two promoters, as these sites are known to be the most significant determinants of expression level in the core promoter[38,39]. Conveniently, these sites are identical between $P_{LtetO-1}$ and $P_{LlacO-1}$, coming from phage lambda P_L in both cases[37]. For each promoter, we constructed all possible single-bp substitutions over this 12bp region (36 mutants for each promoter), along with the wildtype sequence. All 37 sequence variants of the two promoters were combined together, resulting in a plasmid library containing: all 1,296 double-promoter mutants, all 36 single-promoter mutants for each promoter (one promoter is mutated, the other is wildtype) and the full wildtype (both promoters are wildtype). The majority of mutations in the RNA polymerase-binding sites are expected to have little or no effect on repressor binding, and their relative effect on expression should be similar across different inducer concentrations[40,41]. However, one of the -10 bases on $P_{LtetO-1}$ overlaps with a *tet* operator, and three of the -35 bases on $P_{LlacO-1}$ are expected to overlap with a *lac* operator[37] (Extended Data Figure 1), meaning that the effect on expression of mutations at these positions could depend strongly on inducer concentration[42].

The overall structure of the plasmid on which the library is based is shown in Extended Data Figure 1. *araA* and *araB* are divergently expressed from $P_{LtetO-1}$ and $P_{LlacO-1}$ promoters, respectively. These two promoters are separated from each other by a short *bsd* blasticidin S resistance[43] cassette, in order to reduce any physical interactions between them. The presence

of a resistance cassette between the promoters also considerably increased cloning efficiency, as explained below, and *bsd* in particular was chosen for its small size (396 bp ORF), making it possible to sequence both promoters on a single amplicon using paired-end Illumina technology (Extended Data Figure 1). The promoters' repressors, *tetR* and *lacI*, were included on the plasmid.

Plasmid molecules were also intergenically tagged with unique DNA barcodes, similarly to reference[44] (Extended Data Figure 1). These were used to help overcome the problem of PCR and sequencing errors and to increase the precision of mutant fitness estimates by providing many independent frequency trajectories for each mutant (Extended Data Figures 2-4). The barcodes thus also allowed us to account for anomalous lineages containing off-target mutations (present in the initial library) and *de novo* mutations (arising during competition assays). They consist of 20 random nucleotides, split into 4 blocks of 5[45] to avoid the creation of restriction sites used in a later sequencing step: $N_5ATN_5ATN_5ATN_5$. Barcodes were inserted downstream of the *lacI-tetR* cassette, far from the $P_{LtetO-1}$ and $P_{LlacO-1}$ promoters, to avoid any effects on *araA* and *araB* expression, and so are expected to be effectively neutral for fitness (Extended Data Figure 1). Care was taken throughout to avoid loss of library complexity (Extended Data Figure 2), and quality controls were employed at each step of library construction.

The pooled plasmid library was constructed using standard restriction-ligation cloning (Extended Data Figure 1). Due to their short length, promoter sequences could be introduced facing outwards on the 5' ends of PCR primers that were used to amplify a *bsd*[43] blasticidin S-resistance cassette from plasmid pKH1511d ($P_{LtetO-1}$ on forward primers and $P_{LlacO-1}$ on reverse primers). This was done using primer pools with randomised nucleotides at each of the 12 target positions for each promoter. The primers also contained restriction sites on their 5' extremities, allowing the resulting amplicon pool to be ligated into the library backbone,

297 pKH11511c, in the desired orientation. The resulting plasmid library was transformed into
298 DH5α Δ*araBA* and colonies were selected on blasticidin S. This strategy ensured that the
299 occurrence of false-positive colonies from undigested or self-ligated vector was negligible, as
300 a functional *ori* could only come from pKH11511c (the pKH1511d *ori* is *pir*-dependent),
301 while *bsd* was only present in pKH1511d. Due to the use of fully-randomised nucleotides at
302 each target position and the combinatorial way in which variants of the two promoters were
303 cloned together, the expected genotype frequencies in this initial library are: 1/16 for WT,
304 1/192 for each of the 72 single-promoter mutants and 1/2304 for each of the 1,296 double-
305 promoter mutants. With this in mind, an estimated 40,000 colonies were harvested in this step
306 to avoid loss of library complexity. Barcodes were added in a 2nd round of restriction-ligation
307 cloning, introduced *via* a randomised PCR primer. The primer, containing fully-randomised
308 nucleotides at 20 positions, was used to amplify the *bla* β-lactamase gene from plasmid
309 pKD3[46], and the resulting amplicon pool was swapped with the *aadA1*
310 streptomycin/spectinomycin resistance gene in the plasmid library backbone. The primer
311 contains restriction sites on its 5' extremity, one of which is used for this ligation, and another
312 of which allows the barcodes to be moved closer to the mutated promoter region in a later
313 step (see *Barcode-promoter association*). The barcoded plasmid library was again
314 transformed into DH5α Δ*araBA* and colonies were this time selected on ampicillin. False-
315 positive colonies were avoided for the same reason as above, as pKD3 also has a *pir*-
316 dependent *ori*. An estimated 100,000 colonies were harvested during this step, with the vast
317 majority expected to contain a unique barcode. Expected barcode richness was thus: 6,250 for
318 WT, 521 for each single-promoter mutant and 43 for each double-promoter mutant. In a final
319 step, the engineered host strain, MG1655 Δ*araBA* D-ara$^{+/evo}$ Δ*fucK* Δ*lacIZYA*::*cat* D/L-ara^{evo},
320 was transformed with this barcoded plasmid library, and an estimated 600,000 colonies were

harvested after selection on ampicillin. Detailed library creation methods are provided in Supplementary Methods.

Barcode-promoter association

To reveal the $P_{LtetO-1}$ and $P_{LlacO-1}$ promoter sequences linked to each barcode sequence, barcodes were first brought closer to the promoters by excision of the intervening region from the plasmid followed by re-circularisation[44]. PCR-amplification was then used to add the technical sequences necessary for paired-end Illumina MiSeq sequencing of barcode-promoter amplicons[44] (Extended Data Figure 1b; Supplementary Methods). The resulting amplicon library is composed of DNA fragments of the structure: P5 - i5 - N_6 PCR tag - $P_{LtetO-1}$ (rev) - *bsd* (rev) - $P_{LlacO-1}$ - N_{20} plasmid barcode - N_6 PCR tag - i7 - P7, which are ~1 kb in size (close to the size-limit for reliable MiSeq sequencing). 300nt paired-end MiSeq sequencing allowed us to sequence the entire $P_{LtetO-1}$ promoter on Read 1 and the plasmid barcode and entire $P_{LlacO-1}$ promoter on Read 2 (note that Reads 1 and 2 do not overlap). For this, a 600-cycle MiSeq Reagent Kit v3 (Illumina) was used, and DNA was loaded at a concentration of 12pM, with a 20% PhiX DNA spike-in (PhiX Control v3, Illumina). Preliminary quality filtering and demultiplexing by the standard MiSeq software package (Illumina) resulted in an output of > 22M read pairs, giving an expected coverage of > 220X for each plasmid barcode. These read pairs were processed to associate every $P_{LtetO-1}$ - $P_{LlacO-1}$ genotype with its respective barcodes (Supplementary Methods).

Mutant library competition assays

The final mutant library (host strain transformed with barcoded plasmid library) was competed over ~30 mean generations (~3 days) in the presence of L-arabinose and different

concentrations of the inducers, aTc and IPTG. Cell density was kept low during competition (OD_{600} < 0.2) by serial transfer into fresh medium, in order to maintain the culture in exponential phase and to avoid large changes in medium composition. Large volumes of media (100 ml) were used to avoid severe population bottlenecks during serial transfer (> 1 x 10^8 cells each transfer). Plasmid DNA was purified from the culture at several time-points for HiSeq sequencing of plasmid barcodes. Plasmid barcode abundance serves as a proxy for the abundance of cells carrying that particular barcode. The change in frequency over time of a barcode thus provides an estimate of competitive fitness for the lineage carrying that barcode[47]. Since we know the $P_{LtetO-1}$-$P_{LlacO-1}$ sequence associated to each barcode (see *Barcode-promoter association*), this in turn provides us with a distribution of fitness estimates for every mutant. Detailed competition assay methods are provided in Supplementary Methods.

The base competition medium consisted of M9 + 0.1% casamino acids (for basal growth) + 0.03% L-arabinose, with 100 µg/ml ampicillin to select against plasmid loss. A preliminary competition experiment was performed under inducer concentrations of 20 ng/ml aTc and 30 µM IPTG, expected to endow the wildtype with near-maximal fitness (although this was found to be inaccurate). A second round of competition experiments was carried out at a later date and was comprised of three different inducer concentration combinations. One duplicated those of the initial experiment to check reproducibility (Extended Data Figures 3 and 4), and the other two were: 5 ng/ml aTc and no IPTG, and 200 ng/ml aTc and no IPTG. No IPTG was chosen to reduce *araB* expression as much as possible, as the preliminary experiments suggested that the wildtype over-expressed *araB* even in the absence of inducer[48], due to promoter leakiness. The range of aTc was chosen to explore near-minimal and maximal *araA* expression.

Barcode-sequencing of competed mutant library

To track plasmid barcode frequencies throughout the competition experiments, barcodes were PCR-amplified from plasmid DNA in 2 steps, as for *Barcode-promoter association*, to add technical sequences necessary for 100nt overlapping paired-end Illumina HiSeq sequencing (Supplementary Methods). This was performed for time-points t_0, t_1, t_2, t_4, t_6 and t_8 (approximately 0, 4, 9, 19, 29 and 39 mean generations) for the preliminary experiment, and t_1, t_2, t_4 and t_6 for the later experiments. These time-points were chosen with the aim of obtaining precise fitness estimates for both large-effect and small-effect mutations[49]. Preliminary quality filtering and demultiplexing (Integragen, Evry, France) resulted in ~18 M read pairs per time-point per competition experiment, giving, for each point, an expected barcode coverage of ~200X and an expected mutant coverage of >14,000X. Processing of these read pairs is described in Supplementary Methods.

Estimation of competitive fitness and epistasis

We found that competitive fitness was not constant over the course of competition, with, for example, a possible period of physiological adaptation between t_0 and t_2 for certain inducer environments (Extended Data Figure 3). By t_6, a substantial number of lower-fitness mutants begin to escape detection completely, and so to avoid any bias in fitness estimates we consider only the frequency changes between t_2 and t_4 (two time-points). We begin by removing outlier barcodes associated to the wildtype genotype, to avoid any systematic biases coming from inaccurate wildtype estimates. This was done by computing the log ratio of t_4 to t_2 counts for all wildtype barcodes and removing those giving values > 1.5x the inter-quartile range above (below) the upper (lower) quartile. We also removed all barcodes giving

393 < 8 reads at t_2 from our dataset. For every remaining mutant barcode, i, we then estimate its
394 log fitness relative to the wildtype as:

395 $$F_i^{rel} = \frac{\ln\left(\frac{f_i^{t_4}}{\sum f_{wt}^{t_4}}\right) - \ln\left(\frac{f_i^{t_2}}{\sum f_{wt}^{t_2}}\right)}{t_4 - t_2},$$

396 where f_i is the frequency of a mutant barcode, $\sum f_{wt}$ is the total frequency of all wildtype
397 barcodes and $t_4 - t_2$ is the number of mean generations between the two time-points
398 considered (~9). We now estimate log relative fitness of a mutant g, F_g^{rel}, as the median of
399 that of its associated barcodes, $F_{g_i}^{rel}$. We use the median barcode fitness as a fitness estimate
400 for each promoter genotype as a convenient way to filter out the many sources of error in a
401 competition experiment (especially undetected mutations introduced during library
402 construction, *de novo* mutations arising during competition and barcode-promoter
403 misassignments due to PCR and sequencing errors) (Extended Data Figure 3a). The number
404 of eligible barcodes for each promoter genotype ranges from a few to thousands (exact
405 numbers are provided in Supplementary Table 6). Some barcodes disappear from our
406 sequencing sample by t_4, and so are given an F_i^{rel} of *–Inf*. In Env_1 and Env_3, for a very few
407 genotypes this is the case for the majority of their barcodes, and we identify these mutants as
408 being less fit than the wildtype but cannot estimate total/marginal fitness effects or epistasis
409 for them.

410 To estimate the precision of mutant fitness estimates, we used standard bootstrapping of the
411 eligible mutant and wildtype barcodes (n=1,000), each time computing the mutants' fitness,
412 F_g^{rel}, as the median fitness of their associated barcodes, $F_{g_i}^{rel}$. The same 1,000 sets of
413 randomly sampled wildtype barcodes were used as the references for all mutants. The
414 bootstrap distributions were then used to determine significance (empirical 95% confidence)
415 for non-neutrality of total (F_g^{rel}) and marginal (F_g^{marg}) fitness effects, non-zero epistasis,

simple sign epistasis and reciprocal sign epistasis, pairing bootstrap F_g^{rel} estimates by sampled wildtype barcode set when necessary.

The marginal fitness change induced by adding mutation *A* to the genetic background *B* is defined as $F_{A|B}^{marg} = F_{AB}^{rel} - F_B^{rel}$, and epistasis between mutations *A* and *B* is defined as $\varepsilon_{AB} = F_{AB}^{rel} - (F_A^{rel} + F_B^{rel})$[50].

Phenotype-fitness model

We consider a linear metabolic reaction path,

$$S \underset{A}{\rightarrow} X \underset{B}{\rightarrow} Y \underset{C}{\rightarrow} Z \rightarrow \cdots$$

where S is the substrate (L-arabinose) concentration. As shown in references[51,27], for S and Z fixed, the steady-state flux for non-saturated enzymes and the intermediate concentration are respectively given by:

$$\varphi = \frac{1}{1/A + 1/B + \eta} \quad (1)$$

$$Y = D - \frac{\varphi}{1/A + 1/B} \quad (2)$$

where A and B are proportional to the maximum reaction rates provided by each enzyme, η is the inverse of the maximal flux, φ_{max}, as imposed by the fixed pathway steps, and D is a certain function of S and equilibrium constants (see reference[51] for detailed expressions). We note that the flux, φ, is an increasing function of A and B and saturates at φ_{max} for very efficient enzymes A and B, or very high concentrations of them. However, at high fluxes, the hypothesis of unsaturated downstream enzymes breaks down, and a reaction step becomes limiting, such that the concentrations of metabolic intermediates may build up to toxic levels.

To account for such saturation, we extend the model above by considering the full Reversible Michealis-Menten (RMM) form for the step C instead of its first order approximation (similar reasoning applies for longer paths). At steady-state, all reaction speeds must be equal, giving for the third step:

$$\varphi = \frac{\alpha Y - \beta Z}{1 + \gamma Y + \delta Z} \quad (3)$$

where $\alpha, \beta, \gamma, \delta$ are the RMM parameters for C. Equivalently, expressing Y as a function of φ:

$$Y = \frac{\beta Z + (1 + \delta Z)\varphi}{\alpha - \gamma \varphi} \quad (4).$$

We could eliminate Y by combining (2) and (4), Z being fixed, and obtain an exact expression for φ. Note that expression (1) is recovered for $\delta = \gamma = 0$, as this corresponds to the unsaturated case. In the general case, φ would still be an increasing function of A and B and saturate at a certain value, but its expression becomes more complicated.

Instead of using the full expression of φ, we report here an approximation with less parameters, which consistently recovers the monotonicity with A and B, and the limit regimes for unsaturated and saturated downstream steps. For this, we simply keep expression (1) for the flux, and set its saturation by the saturation of the reaction catalysed by C, as obtained in the limit of very high Y in (4):

$$\varphi_{max} = 1/\eta = \alpha/\gamma \, .$$

With this, expression (4) becomes:

$$Y = \frac{P + Q\varphi}{\varphi_{max} - \varphi} \quad (5)$$

where P and Q are functions of the fixed downstream enzyme properties and concentrations. We note in particular that Y diverges when the flux becomes maximal, meaning that the downstream reaction is saturated, leading to an accumulation of Y.

We now assume fitness to be a function of flux and the toxic intermediate (L-ribulose-5-phosphate) concentration, Y, and that there exist constants e and f such that, from (1) and (5):

$$F = e\varphi - fY = e\varphi - f\frac{P + Q\varphi}{\varphi_{max} - \varphi} \quad (6).$$

This expression can be further simplified by considering the low and high flux regimes:

For $\varphi << \varphi_{max}$, (6) behaves as $F = -fP/\varphi_{max} + u\varphi$, with $u = e - f(Q + P/\varphi_{max})/\varphi_{max}$, the offset $-fP/\varphi_{max}$ being determined solely by properties of the fixed downstream enzyme, C. Thus, any fitness change due to mutations in A and B is of the form $u\varphi$.

For $\varphi \sim \varphi_{max}$, the first term of (6) remains finite while the second with numerator $v = f(P + Q\varphi_{max})$ diverges. Thus, replacing e by u as defined in the regime $\varphi << \varphi_{max}$ has a negligible contribution.

Introducing a basal growth rate, ω, supplied by alternative nutrients in the medium (casamino acids), fitness is then well approximated by:

$$F = \omega + u\varphi - \frac{v}{\varphi_{max} - \varphi} \quad (7).$$

In addition to flux and toxic metabolite concentration, gene expression burden can also contribute to fitness changes[28,48,52,53]. Following the observation that protein expression burden depends on metabolic state[54,55], we include an expression cost factor in which θ_A and θ_B describe the cost of increasing cellular enzyme activity, including potential contributions from both the amount of expression and the specific enzyme activity constants:

$$F = \left(\omega + u\varphi - \frac{v}{1/\eta - \varphi}\right)(1 - \theta_A A - \theta_B B) \quad (8).$$

This expression is considered valid only when both factors are positive. Expression (8) defines a fitness surface in the two-dimensional space of AraA and AraB activities, which together with the flux function (1) results in the 6 independent parameters, ω, u, v, θ_A, θ_B and η.

The entire model consists of 83 parameters: the 6 described immediately above; 5 defining the "wildtype" activity levels (AraA and AraB activities for the 3 inducer environments, with Env_2 and Env_3 having the same wildtype AraB activity, as both contained the same IPTG concentration); and 72 defining the relative impact of the single mutations (36 for each gene) on enzyme expression. For a given parameter set, the fitness, F^{rel}, of the 72 single mutants and 1,296 double mutants was computed in each of the 3 environments, relative to the respective "wildtype" fitness. As for the experimental data, the 83-parameter model thus yields 1,368 mutants, each associated to 3 different fitness measurements.

The model was fit using multiple Monte Carlo Markov Chains (MCMC)[56]. Parameters were generated randomly from uniform distributions, both initially and at each step of the chain for a randomly chosen parameter (bounds are provided in Extended Data Figure 8a and Supplementary Table 7; bounds for expression effects of inducer concentrations and a few mutations were guided by experimental expression measurements (data not shown)). 800 chains, each of 300,000 steps, were simulated, and for each chain the parameter set giving the best fit with measured fitness values was stored (residuals were weighted to give equal consideration overall to single and double mutants, and were also normalised to the mean fitness effect in the environment from which they came). The distribution of goodness-of-fit values from the 800 chains was multi-modal (*ie*. convergence was not guaranteed), with ~5-

10% of the chains achieving a best fit residing in the lowest peak. We take the best of all these parameter sets as the most likely fit, but the distributions of parameter values from the best 2.5% of chains are also provided in Extended Data Figure 8a and Supplementary Table 7.

Several fitness function variations containing less parameters than the one presented in the main text were fit in the same way, and we conclude that flux, toxicity and gene expression burden must all be accounted for to explain the observed fitness and epistasis values (Extended Data Figure 9).

Statistical analyses

All statistical analyses were performed in R (v.3.4.3) and figures were made using the R packages ggplot2 and rgl (for the 3D plot). Lower and upper hinges of box plots correspond to the first and third quartiles. Centre line is the median. Upper and lower whiskers extend from the hinges to the largest and lowest value no further than 1.5× the inter-quartile range away, respectively. Points outside this range are plotted individually.

Data availability

All genotype fitness estimates, along with their bootstrap 95% CIs and the number of replicates used to compute them, are provided in Supplementary Table 6. Raw and processed sequencing data has been submitted to GEO (accession number GSE115725).

Code availability

Custom code used in this study is available from the authors upon request.

References

1. DeBerardinis, R. J. & Thompson, C. B. Cellular metabolism and disease: What do metabolic outliers teach us? *Cell* **148,** 1132–1144 (2012).

2. Scriver, C. R. & Waters, P. J. Monogenic traits are not simple: lessons from phenylketonuria. *Trends Genet.* **15,** 267–272 (1999).

3. Badano, J. L. & Katsanis, N. Beyond Mendel: an evolving view of human genetic disease transmission. *Nat. Rev. Genet.* **3,** 779–789 (2002).

4. Manolio, T. A. *et al.* Finding the missing heritability of complex diseases. *Nature* **461,** 747–753 (2009).

5. Cooper, D. N., Krawczak, M., Polychronakos, C., Tyler-Smith, C. & Kehrer-Sawatzki, H. Where genotype is not predictive of phenotype: towards an understanding of the molecular basis of reduced penetrance in human inherited disease. *Hum. Genet.* **132,** 1077–1130 (2013).

6. Argmann, C. A., Houten, S. M., Zhu, J. & Schadt, E. E. A next generation multiscale view of inborn errors of metabolism. *Cell Metab.* **23,** 13–26 (2016).

7. Avery, L. & Wasserman, S. Ordering gene function: the interpretation of epistasis in regulatory hierarchies. *Trends Genet.* **8,** 312–316 (1992).

8. Segrè, D., DeLuna, A., Church, G. M. & Kishony, R. Modular epistasis in yeast metabolism. *Nat. Genet.* **37,** 77–83 (2005).

9. Onge, R. P. S. *et al.* Systematic pathway analysis using high-resolution fitness profiling of combinatorial gene deletions. *Nat. Genet.* **39,** 199–206 (2007).

10. Breslow, D. K. *et al.* A comprehensive strategy enabling high-resolution functional analysis of the yeast genome. *Nat. Methods* **5,** 711–718 (2008).

11. Beltrao, P., Cagney, G. & Krogan, N. J. Quantitative genetic interactions reveal biological modularity. *Cell* **141,** 739–745 (2010).

12. Lehner, B. Molecular mechanisms of epistasis within and between genes. *Trends Genet.* **27,** 323–331 (2011).

13. Fu, C., Deng, S., Jin, G., Wang, X. & Yu, Z.-G. Bayesian network model for identification of pathways by integrating protein interaction with genetic interaction data. *BMC Syst. Biol.* **11,** (2017).

14. Karczewski, K. J. & Snyder, M. P. Integrative omics for health and disease. *Nat. Rev. Genet.* **19,** 299–310 (2018).

15. Schadt, E. E. Molecular networks as sensors and drivers of common human diseases. *Nature* **461,** 218–223 (2009).

16. Zhang, X., Kuivenhoven, J. A. & Groen, A. K. Forward Individualized Medicine from Personal Genomes to Interactomes. *Front. Physiol.* **6,** (2015).

17. Szappanos, B. *et al.* An integrated approach to characterize genetic interaction networks in yeast metabolism. *Nat. Genet.* **43,** 656–662 (2011).

18. Costanzo, M. *et al.* A global genetic interaction network maps a wiring diagram of cellular function. *Science* **353,** aaf1420–aaf1420 (2016).

19. Favé, M.-J. *et al.* Gene-by-environment interactions in urban populations modulate risk phenotypes. *Nat. Commun.* **9,** (2018).

20. Schleif, R. Regulation of the L-arabinose operon of Escherichia coli. *Trends Genet.* **16,** 559–565 (2000).

21. Englesberg, E. *et al.* L-arabinose-sensitive, L-ribulose 5-phosphate 4-epimerase-deficient mutants of Escherichia coli. *J. Bacteriol.* **84,** 137–146 (1962).

22. Poelwijk, F. J., Kiviet, D. J., Weinreich, D. M. & Tans, S. J. Empirical fitness landscapes reveal accessible evolutionary paths. *Nature* **445,** 383–386 (2007).

23. de Visser, J. A. G. M., Cooper, T. F. & Elena, S. F. The causes of epistasis. *Proc. R. Soc. B Biol. Sci.* **278,** 3617–3624 (2011).

24. Berger, D. & Postma, E. Biased Estimates of Diminishing-Returns Epistasis? Empirical Evidence Revisited. *Genetics* **198,** 1417–1420 (2014).

25. Dykhuizen, D. E., Dean, A. M. & Hart, D. L. Metabolic flux and fitness. *Genetics* **115,** 25–31 (1987).

26. Clark, A. G. Mutation-selection balance and Metabolic Control Theory. *Genetics* **129,** 909–923 (1991).

27. Szathmary, E. Do deleterious mutations act synergistically? Metabolic Control Theory provides a partial answer. *Genetics* **133,** 127–132 (1993).

28. Dekel, E. & Alon, U. Optimality and evolutionary tuning of the expression level of a protein. *Nature* **436,** 588–592 (2005).

29. Orth, J. D., Thiele, I. & Palsson, B. Ø. What is flux balance analysis? *Nat. Biotechnol.* **28,** 245–248 (2010).

30. Blanquart, F., Achaz, G., Bataillon, T. & Tenaillon, O. Properties of selected mutations and genotypic landscapes under Fisher's Geometric Model. *Evolution* **68,** 3537–3554 (2014).

31. Leblanc, D. J. & Mortlock, R. P. The metabolism of d-arabinose: Alternate kinases for the phosphorylation of d-ribulose in Escherichia coli and Aerobacter aerogenes. *Arch. Biochem. Biophys.* **150,** 774–781 (1972).

32. LeBlanc, D. J. & Mortlock, R. P. Metabolism of D-Arabinose: Origin of a D- Ribulokinase Activity in Escherichia coli. *J. Bacteriol.* **106,** 82–89 (1971).

33. LeBlanc, D. J. & Mortlock, R. P. Metabolism of D-Arabinose: a New Pathway in Escherichia coli. *J. Bacteriol.* **106,** 90–96 (1971).

34. Fritz, G. *et al.* Single Cell Kinetics of Phenotypic Switching in the Arabinose Utilization System of E. coli. *PLoS ONE* **9,** e89532 (2014).

35. Khlebnikov, A. & Keasling, J. D. Effect of lacY Expression on Homogeneity of Induction from the Ptac and Ptrc Promoters by Natural and Synthetic Inducers. *Biotechnol. Prog.* **18,** 672–674 (2002).

598 36. Wray, G. A. The evolutionary significance of cis-regulatory mutations. *Nat. Rev. Genet.* **8,**
599 206–216 (2007).

600 37. Lutz, R. Independent and tight regulation of transcriptional units in Escherichia coli via the
601 LacR/O, the TetR/O and AraC/I1-I2 regulatory elements. *Nucleic Acids Res.* **25,** 1203–1210 (1997).

602 38. Shultzaberger, R. K., Malashock, D. S., Kirsch, J. F. & Eisen, M. B. The Fitness Landscapes of
603 cis-Acting Binding Sites in Different Promoter and Environmental Contexts. *PLoS Genet.* **6,** e1001042
604 (2010).

605 39. Kinney, J. B., Murugan, A., Callan, C. G. & Cox, E. C. Using deep sequencing to characterize
606 the biophysical mechanism of a transcriptional regulatory sequence. *Proc. Natl. Acad. Sci.* **107,**
607 9158–9163 (2010).

608 40. Brewster, R. C., Jones, D. L. & Phillips, R. Tuning Promoter Strength through RNA Polymerase
609 Binding Site Design in Escherichia coli. *PLoS Comput. Biol.* **8,** e1002811 (2012).

610 41. Bintu, L. *et al.* Transcriptional regulation by the numbers: models. *Curr. Opin. Genet. Dev.* **15,**
611 116–124 (2005).

612 42. Lagator, M., Paixão, T., Barton, N. H., Bollback, J. P. & Guet, C. C. On the mechanistic nature
613 of epistasis in a canonical cis-regulatory element. *eLife* **6,** (2017).

614 43. Kimura, M., Takatsuki, A. & Yamaguchi, I. Blasticidin S deaminase gene from Aspergillus
615 terreus (BSD): a new drug resistance gene for transfection of mammalian cells. *Biochim. Biophys.*
616 *Acta* **1219,** 653–659 (1994).

617 44. Sarkisyan, K. S. *et al.* Local fitness landscape of the green fluorescent protein. *Nature* **533,**
618 397–401 (2016).

619 45. Levy, S. F. *et al.* Quantitative evolutionary dynamics using high-resolution lineage tracking.
620 *Nature* **519,** 181–186 (2015).

621 46. Datsenko, K. A. & Wanner, B. L. One-step inactivation of chromosomal genes in Escherichia
622 coli K-12 using PCR products. *Proc. Natl. Acad. Sci.* **97,** 6640–6645 (2000).

623 47. Hietpas, R. T., Jensen, J. D. & Bolon, D. N. A. Experimental illumination of a fitness landscape.
624 *Proc. Natl. Acad. Sci.* **108,** 7896–7901 (2011).

625 48. Chou, H.-H., Delaney, N. F., Draghi, J. A. & Marx, C. J. Mapping the fitness landscape of gene
626 expression uncovers the cause of antagonism and sign epistasis between adaptive mutations. *PLoS*
627 *Genet.* **10,** e1004149 (2014).

628 49. Matuszewski, S., Hildebrandt, M. E., Ghenu, A.-H., Jensen, J. D. & Bank, C. A Statistical Guide
629 to the Design of Deep Mutational Scanning Experiments. *Genetics* **204,** 77–87 (2016).

630 50. Beyond the Average: The Evolutionary Importance of Gene Interactions and Variability o f
631 Epistatic Effects. in *Epistasis and the Evolutionary Process* (eds. Wolf, J. B., Brodie III, E. D. & Wade,
632 M. J.) 10 (Oxford University Press, 2000).

633 51. Kacser, H. & Burns, J. A. The Molecular Basis Of Dominance. *Genetics* **97,** 639–666 (1981).

634 52. Nguyen, T. N. M., Phan, Q. G., Duong, L. P. & Bertrand, K. P. Effects of carriage and
635 expression of the Tn10 tetracycline-resistance operon on the fitness of Escherichia coli K12. *Mol.*
636 *Biol. Evol.* **6,** 213–225 (1989).

637 53. Koch, A. L. The protein burden of lac operon products. *J. Mol. Evol.* **19,** 455–462 (1983).

638 54. Bienick, M. S. *et al.* The Interrelationship between Promoter Strength, Gene Expression, and
639 Growth Rate. *PLoS ONE* **9,** e109105 (2014).

640 55. Kafri, M., Metzl-Raz, E., Jona, G. & Barkai, N. The Cost of Protein Production. *Cell Rep.* **14,**
641 22–31 (2016).

642 56. Brroks, S., Gelman, A., Jones, G. L. & Meng, X.-L. *Handbook of Markov Chain Monte Carlo*.
643 (Chapman and Hall/CRC, 2011).

644

645 **Extended data** is linked to this paper.

646 **Supplementary Information** is linked to this paper.

647 **Acknowledgements** We thank A. Birgy, A. Decrulle, I. Matic, M. Deyell, A. Soler and D. Mazel for
648 providing genetic material and technical advice, A. Baron, J. Chatel, A. Bridier-Nahmias and the
649 CRI cytometry facility for technical assistance, and L.-M. Chevin, B. Gaut and E. Denamur for
650 critical reading of the manuscript. MiSeq sequencing was performed using equipment provided by the
651 Genetics Department of Bichat-Claude Bernard Hospital. This work was supported by the European
652 Research Council under the European Union's Seventh Framework Programme (ERC grant 310944 to
653 O.T.). H.K. was supported by the Ecole Doctorale Frontières du Vivant (FdV) – Programme
654 Bettencourt.

655 **Author Contributions** H.E.K., P.N. and O.T. conceived the idea for the experiment; H.E.K. and O.T.
656 designed the experiments; H.E.K., C.E., A.C., A.E.C., M.A.M., G.G. and H.L.N. performed the
657 experiments; H.E.K., P.N. and O.T. performed the analyses; H.E.K., P.N. and O.T. wrote the paper.

658 **Author Information** The authors declare no competing financial interests. Correspondence and
659 requests for materials should be addressed to O.T. (olivier.tenaillon@inserm.fr).

660

661

662

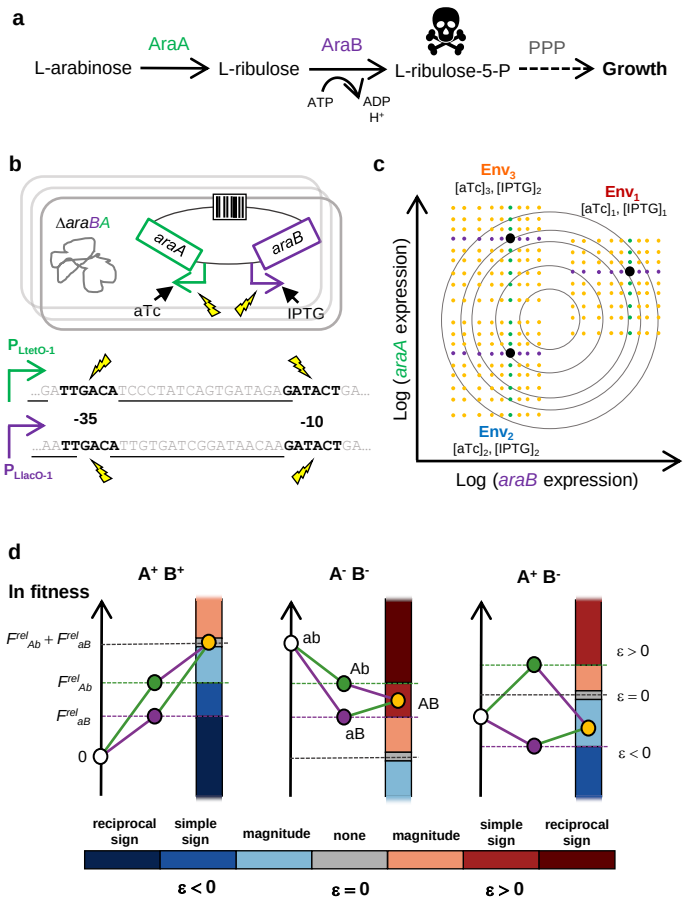

Figure 1. High-throughput, quantitative mapping of fitness interactions between expression variants of two metabolic genes in different expression-modifying environments. a, L-arabinose pathway of *E. coli*. **b**, *araA* and *araB* were each placed under the control of an artificial inducible promoter, making their expression sensitive to the concentration of their respective inducers, anhydrotetracycline (aTc) and isopropyl β-D-1-thiogalactopyranoside (IPTG). A barcoded library of mutant promoter combinations was then constructed, with mutagenesis targeted in the -35 and -10 RNA-polymerase binding hexamers (black letters). Underlined bases are annotated repressor binding sites. **c**, Competitive fitness was measured under different inducer concentrations defining three environments. $P_{LtetO-1}$ single mutants – green; $P_{LlacO-1}$ single mutants – purple; double mutants - orange. Contours are hypothetical fitness isoclines. **d**, Epistasis was quantified for all mutant promoter pairs across environments. Epistasis can be categorised as either *magnitude* or *sign* type. *Sign epistasis* can be further categorised as *simple* (effect of *one* mutation changes sign in presence of the other) or *reciprocal* (effects of *both* mutations change sign in the presence of the other). Capitalised letters represent mutant alleles of $P_{LtetO-1}$-*araA* and $P_{LlacO-1}$-*araB*. Superscript plus and minus denote that individual alleles are beneficial or deleterious, respectively.

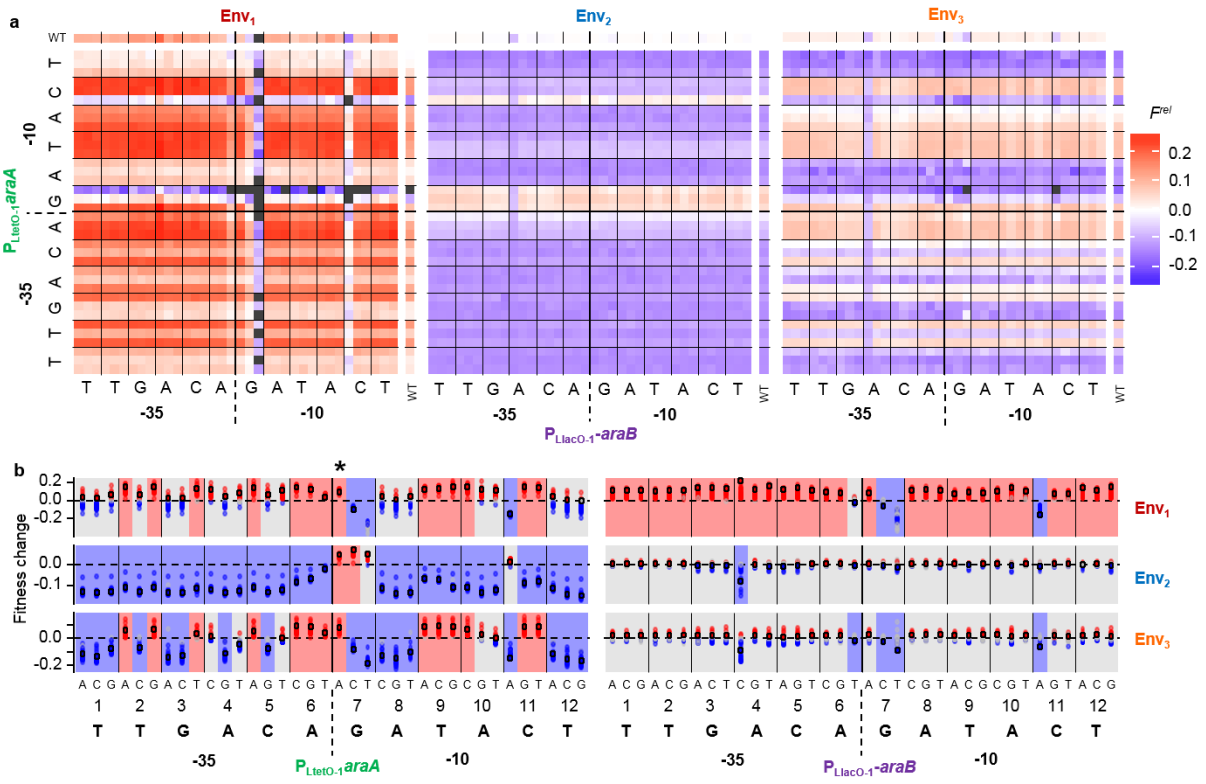

Figure 2. Fitness effects of promoter mutations in different backgrounds and environments. a, Genotypes are coloured according to the natural logarithm of their fitness relative to the wildtype (F^{rel}). Grey denotes unquantifiable fitness effects. "-35" and "-10" denote the RNA polymerase-binding hexamers. Letters show the wildtype base at each position, and the 3 mutations at each position are ordered alphabetically, as in **b**. F^{rel} of single promoter mutants is shown in the right-most column (for *araA*) and the top row (for *araB*), with the rest of the maps showing that of the corresponding double mutants. Inducer concentrations were: 20 ng/ml aTc and 30 µM IPTG (Env_1); 5 ng/ml aTc and no IPTG (Env_2); 200 ng/ml aTc and no IPTG (Env_3). **b,** Fitness changes when an allele of one promoter is added to alleles of the second promoter. Large outlined points indicate that the "background" promoter is wildtype. Red, blue and grey points indicate positive, negative and non-significant fitness changes, respectively. Red, blue and grey rectangles indicate that, in a given environment, an allele can be beneficial but never deleterious, deleterious but never beneficial, or both beneficial and deleterious. G7A of $P_{LtetO-1}$-*araA* (*) is the only allele conferring a qualitatively consistent fitness effect (beneficial) across all backgrounds and environments.

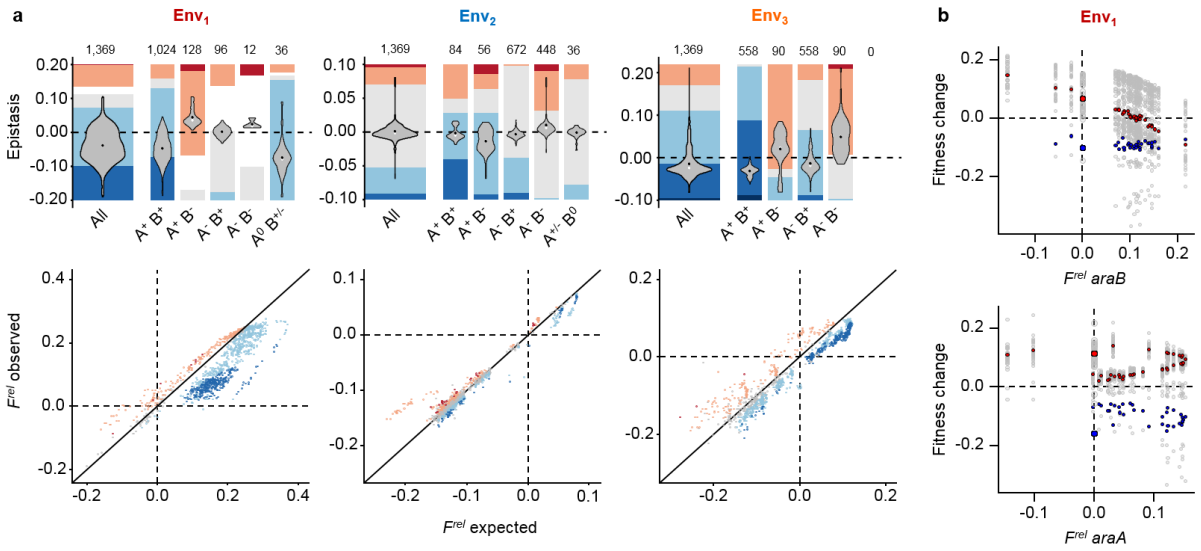

Figure 3. Strength, types and trends of epistasis in different environments. a, Violins show distribution of epistasis for different kinds of mutation pairs (white and black points show median and mean, respectively). Mutation pairs may be composed of mutations that are individually both beneficial (A^+ B^+), both deleterious (A^- B^-) or mixed (A^+ B^- and A^- B^+), or one of which confers an undetectable fitness effect on its own (A^0 $B^{+/-}$ and $A^{+/-}$ B^0). The number of each such pair is shown above violins. Stacked bars show the fraction of different epistasis types detected (colours as in Fig. 1d, with white for pairs for which epistasis could not be computed). Scatterplots show fitness of double mutants against that expected if mutation effects combined additively. Points coloured as in Fig. 1d. **b,** Relationship between background fitness and the fitness change induced by introducing a mutation in the second promoter, in Env_1. Top: *araA* promoter mutations added to existing *araB* promoter mutations; bottom: inverse case. Coloured points highlight particular alleles. Top: $P_{LtetO\text{-}1}$-*araA* alleles T2C (red) and G7C (blue). Bottom: $P_{LlacO\text{-}1}$-*araB* alleles T1A (red) and C11A (blue). Large points show effect of alleles in the wildtype background.

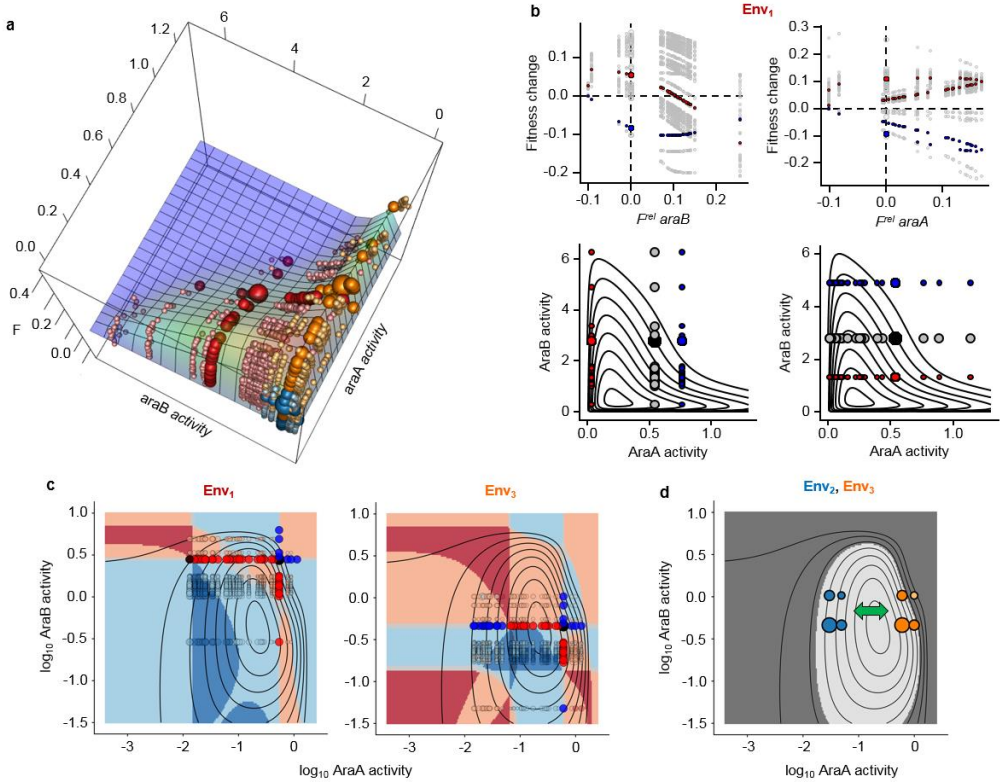

Figure 4. Mechanistic basis of heterogeneous, environmentally dependent intergenic epistasis. a, Surface shows fitted activity-fitness model. Spheres are positioned according to predicted activity levels and *observed* relative fitness (Env_1 – red; Env_2 – blue; Env_3 - orange). Three largest spheres are wildtype, intermediate-sized spheres are single mutants, and small, pale spheres are double mutants. **b**, Upper plots recapitulate Fig. 3b, with fitness values predicted by the model. Lower plots show predicted position in the fitness landscape of highlighted genotypes from upper plots (black point is wildtype; other large points are single mutants, grey for the gene considered to be carrying the "background" alleles). **c**, Fitness surface shown on log activity scale. Intergenic epistasis types emerging from model are indicated by surface colour (colours as in Fig. 1d). Predicted epistasis is determined as non-significant (grey) if magnitude is less than 0.005. Large black points are wildtype. Smaller, opaque blue, red and black points are single mutants, coloured by *observed* F^{rel} (deleterious, beneficial and neutral, respectively). Transparent points are double mutants, coloured by observed epistasis type and sized by epistasis strength. **d,** Dark grey area is a hypothetical disease threshold, at 40% of maximum fitness. Points show four genotypes in Env_2 (blue) and Env_3 (orange): the wildtype (largest), C11A of $P_{LtetO-1}$-*araA* and G7T of $P_{LlacO-1}$-*araB* (intermediate size), and the resulting double-mutant (smallest). Green arrow represents a change in enzyme activity levels caused by non-genetic factors like ageing or environmental exposure, or by further mutations. A toxicity-induced disease state results here from one particular combination of alleles and environment (pale orange point).